

**IMPROVED PREDICTION OF COASTAL
FLOODING DUE TO TROPICAL CYCLONES:
AN INTEGRATED MODELLING APPROACH
FOR THE EAST COAST OF INDIA**

Pawan Tiwari



**CENTRE FOR ATMOSPHERIC SCIENCES
INDIAN INSTITUTE OF TECHNOLOGY DELHI**

March 2026

©Indian Institute of Technology Delhi (IITD), New Delhi, 2026

**IMPROVED PREDICTION OF COASTAL
FLOODING DUE TO TROPICAL CYCLONES:
AN INTEGRATED MODELLING APPROACH
FOR THE EAST COAST OF INDIA**

by

Pawan Tiwari

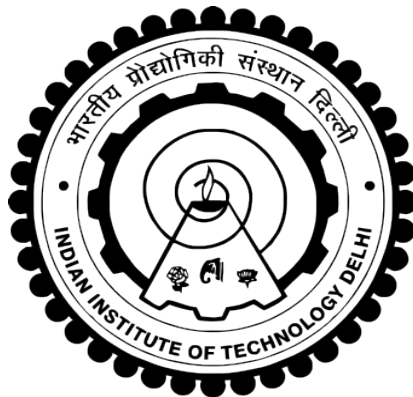
Centre for Atmospheric Sciences

Submitted

in fulfilment of the requirements of the degree of

DOCTOR OF PHILOSOPHY

to the



INDIAN INSTITUTE OF TECHNOLOGY DELHI

March 2026

Dedicated to my parents

Certificate

This is to certify that the thesis entitled "**Improved Prediction of Coastal Flooding due to Tropical Cyclones: An Integrated Modelling Approach for the East Coast of India**" being submitted by **Mr. Pawan Tiwari** to the Indian Institute of Technology Delhi for the award of the degree of **DOCTOR OF PHILOSOPHY** is a record of original bonafide research carried out by him. Mr. Pawan has worked under my guidance and supervision and has fulfilled the requirements for the submission of this thesis. The results contained in this thesis have not been submitted in part or full to any other University or Institute for the award of any degree or diploma.

(Dr A. D. Rao)

Emeritus Professor (Retd.),
Centre for Atmospheric Sciences,
Indian Institute of Technology Delhi,
New Delhi-110016.

(Dr Vimlesh Pant)

Professor,
Centre for Atmospheric Sciences,
Indian Institute of Technology Delhi,
New Delhi-110016.

Acknowledgements

The pursuit of a doctoral degree is a journey filled with uncertainty, challenge, and the excitement of discovery. Reaching this stage of completing my PhD thesis evokes memories of moments both exhilarating and overwhelming times of inspiration as well as instances of doubt and exhaustion. Yet, amid these contrasting experiences, there were invisible forces of positivity and enlightenment that guided me forward, often turning despair into motivation and confusion into clarity. I humbly bow to that unseen energy and divine grace that illuminated my path and sustained me through every phase of this journey.

I express my sincere and profound gratitude to my supervisors, Prof. A. D. Rao and Prof. Vimlesh Pant, for their invaluable guidance, encouragement, and unwavering support throughout my doctoral research. I am deeply indebted to Prof. A. D. Rao for his insightful supervision, progressive vision, and constant motivation that kept me inspired through every phase of this journey. His immense knowledge, clarity of thoughts, and unmatched enthusiasm towards research and life have always encouraged me to push boundaries and explore ideas beyond the conventional domain. His mentorship extended beyond academics, shaping my way of thinking and instilling in me a sense of perseverance and curiosity. I also extend my heartfelt thanks to Prof. Vimlesh Pant, for his thoughtful guidance, constructive suggestions, and consistent encouragement, which significantly enriched the depth and direction of this work. Their combined mentorship created an intellectually stimulating and supportive environment that made this journey both fulfilling and transformative, for which I remain sincerely grateful.

I sincerely thank the members of my Student Research Committee (SRC): Prof. Somnath Baidya Roy (Chair), Prof. Sarvesh Dubey, and Prof. Bhaskar Kanseri for their valuable time, insightful comments, and constructive suggestions that greatly improved the quality of my work. I am also grateful to Prof. Samiran Mandal for his continuous support and scientific inputs, which contributed meaningfully to the progress of my work. My heartfelt thanks to Prof. Sagnik Dey, Head, Centre for Atmospheric Sciences (CAS), for his encouragement, guidance, and for creating an inspiring academic environment conducive to research.

I owe my deepest gratitude to my parents, Mrs. Shakuntala Tiwari and Shri Ramkesh Tiwari, whose unconditional love, constant encouragement, and sacrifices have been the foundation of all my achievements. Their faith in me has been my greatest strength, and their values have guided me through every stage of life. This accomplishment is as much theirs as it is mine, and I dedicate this work to them with heartfelt love and respect. I am sincerely grateful to my dear

siblings, Anil, Suneil, and Khushboo, for their constant encouragement, understanding, and unwavering support throughout my journey. Their belief in me has always been a source of motivation and strength. I am also deeply thankful to my family members Rahul, Meena, Reena, Neha, Priti, Vivek, Priya and Abhishek. Their support provided the emotional grounding that helped me persevere through every challenge. I would also like to express my affection and appreciation to my nephew Harshit and my nieces Maanvi and Riddhi, whose joy and warmth have brought happiness and positivity throughout this journey.

I would like to express my special thanks to Dr. Smita Pandey for her continuous support, guidance, and encouragement right from the very beginning of my PhD journey. Her timely advice, patience, and motivation have been invaluable in shaping the progress of my research. I am also sincerely grateful to Dr. P. L. N. Murty for his kind support, helpful suggestions, and assistance, which significantly contributed to the smooth completion of this work.

I am grateful to my friends Sankar, Subhojit, Chiranjit, Anna, Pragnya, Ajay and Damini who have been like family throughout this journey. Their constant encouragement, camaraderie, and support made the challenges of the PhD journey lighter and the achievements even more memorable.

I express my gratitude to my seniors Dr. Badarvada Yadidya, Dr. Vivek Seelanki, Dr. Naveen Chandra, Dr. Anasuya, and Kunal for their guidance, advice, and support throughout my doctoral journey. Their experience, encouragement, and willingness to share knowledge provided valuable insights and helped me navigate the challenges of research with confidence. I thank my lab mates Suraj, Arun, Anna, Rajesh, Riyaz, and Arnab for their constant support, cooperation, and camaraderie in the laboratory and during various research activities.

My sincere thanks go to all the supportive and friendly staff of the CAS, library, administration, and HPC facility for providing resources and assistance that made it easier to focus on my research goals. Finally, there are numerous people, both directly and indirectly, whose help and support were invaluable, and I convey my heartfelt thanks to all friends and well-wishers who contributed in any way to the completion of this work.

Pawan Tiwari

New Delhi

Abstract

Tropical cyclones (TC) pose a significant threat to the densely populated coastal areas due to generation of storm surges (SS) and associated inundation. This threat becomes even more severe in deltaic regions, particularly when a cyclone crosses a river estuary, leading to compound flooding (CF) caused by the combined effects of downstream storm tide (ST), precipitation (Pcp), and upstream river discharge (RD). The thesis presents a comprehensive investigation into cyclone-induced SS and associated inland flooding along the east coast of India using a fully coupled hydrodynamic Advanced CIRCulation (ADCIRC), wave Simulating Wave nearshore (SWAN) and hydraulic Hydrologic Engineering Center's River Analysis System (HEC-RAS) models.

A standalone high-resolution ADCIRC model with 100 m nearshore resolution and 18 km in the open ocean is set-up along the east coast of India for the computation of SS and associated inundation. The model water elevations are validated well at various tide-gauge locations. A directional surface roughness parameterization is implemented to represent spatially varying wind and bottom stress derived from land use and land cover (LULC) data. The ERA5 reanalysis indicates that cyclonic winds over the coastal land are weaker by 29–50% compared to adjacent oceans during landfall period. A comparison of cyclonic wind speed after incorporating LULC data in the model is made with an automatic surface observation system (ASOS). It suggests about 15–29% reduction in the wind speed, which is consistent with ASOS. The inundated area computed for the cyclones advocates a significant reduction of about 15–50% due to LULC. Further, sensitivity experiments are performed to examine the impact of mangroves in the Krishna estuary located in between two concave-shaped coastal geometries. Replacing wetlands with Mangroves in the Krishna estuary region results in a

simultaneous decline in the wind speed (12.5%) and inundated area (13.4%). It also highlights that bottom friction contributes (9.4%) in the inundated area against surface friction (4%). These findings underscore the crucial role of vegetation and land cover in mitigating cyclone-induced flooding and support the need for coastal ecosystem restoration and management.

The shape of the coastline, whether concave or convex, significantly influences the generation and propagation of SS during any extreme weather events like TC. A comprehensive investigation is made on the generation of SS along the coast in response to complex coastline geometry using a standalone ADCIRC model. The study deals with sensitivity experiments by using various idealized concave/convex model domains with the same intensity of parallel cyclone tracks. It demonstrates that a sharp curvature along with the landfall location of each track within the domain has more influence on the surge evolution. Peak surges (PS) are generated in the domain for the tracks possessing strong onshore winds, while intense alongshore winds are responsible for PS spreading along the coast. The propagation of energy density per unit length associated with surge waves is computed for concave coasts to explain the funneling effect. Development of PS is also seen with actual intricate coastal stretch having concave and convex coastlines along the east coast of India using parallel tracks, which is consistent with that of idealized experiments. Further simulations are carried out with real coastline with different approach angles of the track exhibit that maximum PS are not always aligned to the east of the track. Depending on approaching track angle, PS may also develop on the west side. Experiments with real coastline also indicate that PS in the concave coastline is more influenced by cyclone's radius of maximum winds. Surge generation with different radius of maximum winds is seen to the west side of the track though the cyclone is not making its landfall in this region. Simulation with a recent cyclone, Michaung reveals that occurrence of ST is also seen to west of the landfall as the track moves parallel to

the coast, which agrees with the observations. This study signifies importance of local coastline configuration, particularly in the concave coasts, on the intensification of SS.

CF in any deltaic region is caused by complex interactions between ST, RD, and Pcp, in which impact of land-surface parameters is often undetermined. A coupled hydraulic HEC-RAS and hydrodynamic ADCIRC model is used to examine how land surface characteristics affect CF during Yaas cyclone. The model includes Brahmani, Baitarani, Subarnarekha, and Mahanadi River tributaries along east coast of India. CF is estimated using IMDAA, ERA5, GPM Pcp, evaporation, along with soil infiltration. Validation of inundation extent with satellite imagery suggests that Pcp is the leading cause of CF. As infiltration rate primarily depends on soil conservation service curve number (SCN) and minimum infiltration rate, sensitivity analysis shows that minimum soil infiltration and maximum SCN increase flooding due to lesser water penetration and higher runoff. Experiments are carried out to calibrate district-wise inundation with the observations by considering suitable minimum infiltration rates and SCN values, leading to 50% increase in CF. Additional simulations with two more historical cyclones (Odisha Super cyclone and Phailin) demonstrate that incorporation of Pcp doubles the inundation compared to RD and ST forcing. The work enlightens significance of various responsible factors for CF along with uncertainties involved in it and emphasizes potential solutions to improve it further.

The relative contributions of different drivers of CF and their interaction with land-surface processes are still unclear, especially in different seasons along with basin morphology. Conventional hydrodynamic models commonly isolate their representation due to lack of Pcp data resulting in underprediction of inundation. To fill this gap, a fully coupled hydraulic, hydrodynamic and wind wave (ADCIRC+SWAN+HEC-RAS) modelling framework is utilized over three major river networks along the east coast of India: Hooghly, Mahanadi–

Brahmani–Baitarani–Subarnarekha, and Krishna–Godavari basins, to quantify the combined influences of ST, RD, Pcp, and surface processes on CF. This is the first study in a multi-basin and seasonally stratified ocean during pre- and post-monsoon cyclone period along the coast. Simulations show that model winds and total water elevations match with the observations. The study shows that pre-monsoon CF is mainly caused by Pcp, but post-monsoon CF is a compound effect of high RD, Pcp, and ST. Further, sensitivity analysis depicts that accurate representation of river cross-sectional data is very critical, while default topographic datasets tend to overestimate flood extents. Inclusion of soil infiltration dynamics in the model reduces inundated area by 30–38%, and hence imperative to be considered in real-time simulations. It also reveals a standalone ADCIRC+SWAN underestimates total flooding by 47% due to the non-inclusion of RD and Pcp, compared to the fully coupled approach emphasizing the need of fully integrated modelling. Study also highlights constraints related to the data and methodological issues and uncertainties associated with fully coupled framework and possible ways to reduce it.

Overall, the thesis provides a multi-scale assessment of cyclone-induced flooding along the Indian east coast. It advances the understanding of how surface and bottom stress, coastline configuration, land-surface characteristics, and multi-driver interactions shape the spatial and temporal evolution of inundation. The findings have strong implications for coastal zone management, disaster preparedness, and the development of resilient coastal infrastructure in cyclone-prone regions.

सारांश

उष्णकटिबंधीय चक्रवात (टी. सी.) तूफान के उछाल (एस. एस.) और संबंधित बाढ़ के कारण घनी आबादी वाले तटीय क्षेत्रों के लिए एक महत्वपूर्ण खतरा पैदा करते हैं। यह खतरा डेल्टा क्षेत्रों में और भी गंभीर हो जाता है, विशेष रूप से जब एक चक्रवात नदी के मुहाने को पार करता है, जिससे डाउनस्ट्रीम स्टॉर्म टाइड (एसटी) वर्षण (पीसीपी) और अपस्ट्रीम नदी निर्वहन (आरडी) के संयुक्त प्रभावों के कारण यौगिक बाढ़ (सीएफ) हो जाती है यह शोध प्रबंध पूरी तरह से युग्मित हाइड्रोडायनामिक एडवांस्ड सीआईआरक्यूलेशन (एडीसीआईआरसी) वेव सिमुलेंटिंग वेव नियरशोर (एसडब्ल्यूएन) और हाइड्रोलिक हाइड्रोलॉजिकल इंजीनियरिंग सेंटर के नदी विश्लेषण प्रणाली (एचईसी-आरएस) मॉडल का उपयोग करके भारत के पूर्वी तट के साथ चक्रवात-प्रेरित एसएस और संबंधित अंतर्देशीय बाढ़ की एक व्यापक जांच प्रस्तुत करता है।

एसएस और संबंधित बाढ़ की गणना के लिए भारत के पूर्वी तट के साथ 100 मीटर निकट तटीय रिज़ॉल्यूशन और खुले महासागर में 18 किमी के साथ एक स्टैंडअलोन उच्च-रिज़ॉल्यूशन एडीसीआईआरसी मॉडल स्थापित किया गया है। मॉडल जल ऊंचाई को विभिन्न ज्वार-गज स्थानों पर अच्छी तरह से मान्य किया जाता है। भूमि उपयोग और भूमि आवरण (एल. यू. एल. सी.) डेटा से प्राप्त स्थानिक रूप से भिन्न हवा और निचले तनाव का प्रतिनिधित्व करने के लिए एक दिशात्मक सतह खुरदरापन पैरामीटराइजेशन लागू किया जाता है। ईआरएस के पुनर्मूल्यांकन से संकेत मिलता है कि तटीय भूमि पर चक्रवाती हवाएं लैंडफॉल अवधि के दौरान निकटवर्ती महासागरों की तुलना में 29-50% तक कमजोर होती हैं। मॉडल में एल्यूएस डेटा को शामिल करने के बाद चक्रवाती हवा की गति की तुलना एक स्वचालित सतह अवलोकन प्रणाली (एसओएस) के साथ की जाती है यह हवा की गति में लगभग 15-29% की कमी का सुझाव देता है, जो ASOS के अनुरूप है। चक्रवातों के लिए गणना किया गया जलमग्न क्षेत्र एल्यूएस के कारण लगभग 15-50% की महत्वपूर्ण कमी की वकालत करता है। इसके अलावा, दो अवतल आकार की तटीय ज्यामिति के बीच स्थित कृष्णा मुहाने में मैंग्रोव के प्रभाव की जांच करने के लिए संवेदनशीलता प्रयोग किए जाते हैं। कृष्णा नदी के मुहाने वाले क्षेत्र में आर्द्रभूमि को मैंग्रोव में बदलने से हवा की गति (12.5%) और जलमग्न क्षेत्र (13.4%) में एक साथ गिरावट आती है यह इस बात पर भी प्रकाश डालता है कि सतह के घर्षण (4%) के खिलाफ जलमग्न क्षेत्र में नीचे का घर्षण योगदान (9.4%) देता है। ये निष्कर्ष चक्रवात-प्रेरित बाढ़

को कम करने में वनस्पति और भूमि आवरण की महत्वपूर्ण भूमिका को रेखांकित करते हैं और तटीय पारिस्थितिकी तंत्र की बहाली और प्रबंधन की आवश्यकता का समर्थन करते हैं।

तटरेखा का आकार, चाहे अवतल हो या उत्तल, टीसी जैसी किसी भी चरम मौसम की घटनाओं के दौरान एसएस के उत्पादन और प्रसार को महत्वपूर्ण रूप से प्रभावित करता है। एक स्टैंडअलोन एडीसीआईआरसी मॉडल का उपयोग करके जटिल तटरेखा ज्यामिति के जवाब में तट के साथ एसएस की पीढ़ी पर एक व्यापक जांच की जाती है। अध्ययन समानांतर चक्रवात पटरियों की समान तीव्रता के साथ विभिन्न आदर्श अवतल/उत्तल मॉडल डोमेन का उपयोग करके संवेदनशीलता प्रयोगों से संबंधित है। यह दर्शाता है कि क्षेत्र के भीतर प्रत्येक ट्रैक के लैंडफॉल स्थान के साथ एक तेज वक्रता का वृद्धि विकास पर अधिक प्रभाव पड़ता है। तटवर्ती हवाओं वाली पटरियों के लिए क्षेत्र में पीक सर्ज (पीएस) उत्पन्न होते हैं, जबकि तीव्र तटवर्ती हवाएं तट के साथ पीएस फैलाने के लिए जिम्मेदार होती हैं। ज्वारीय तरंगों से जुड़े प्रति इकाई लंबाई के ऊर्जा घनत्व के प्रसार की गणना अवतल तटों के लिए फ़नेलिंग प्रभाव की व्याख्या करने के लिए की जाती है। पीएस का विकास समानांतर पटरियों का उपयोग करके भारत के पूर्वी तट के साथ अवतल और उत्तल तटरेखा वाले वास्तविक जटिल तटीय खंड के साथ भी देखा जाता है, जो आदर्श प्रयोगों के अनुरूप है। ट्रैक के विभिन्न दृष्टिकोण कोणों के साथ वास्तविक तटरेखा के साथ आगे सिमुलेशन किए जाते हैं जो दर्शाते हैं कि अधिकतम पीएस हमेशा ट्रैक के पूर्व में संरेखित नहीं होते हैं। निकटवर्ती ट्रैक कोण के आधार पर, पीएस पश्चिम की ओर भी विकसित हो सकता है। वास्तविक तटरेखा के साथ प्रयोगों से यह भी संकेत मिलता है कि अवतल तटरेखा में पीएस चक्रवात की अधिकतम हवाओं की त्रिज्या से अधिक प्रभावित होता है। ट्रैक के पश्चिम की ओर अधिकतम हवाओं के विभिन्न त्रिज्या के साथ सर्ज जनरेशन देखा जाता है, हालांकि चक्रवात इस क्षेत्र में अपना लैंडफॉल नहीं बना रहा है। हाल के एक चक्रवात के साथ अनुकरण, माइकॉन से पता चलता है कि एसटी की घटना को लैंडफॉल के पश्चिम में भी देखा जाता है क्योंकि ट्रैक तट के समानांतर चलता है, जो टिप्पणियों से सहमत है। यह अध्ययन स्थानीय तटरेखा विन्यास के महत्व को दर्शाता है, विशेष रूप से अवतल तटों में, तूफान के बढ़ने की तीव्रता पर।

किसी भी डेल्टा क्षेत्र में सी. एफ. एस. टी., आर. डी. और पी. सी. पी. के बीच जटिल अंतःक्रियाओं के कारण होता है, जिसमें भूमि-सतह मापदंडों का प्रभाव अक्सर अनिर्धारित होता है। एक युग्मित हाइड्रोलिक एच. ई. सी.-आर. ए. एस. और

हाइड्रोडायनामिक ए. डी. सी. आई. आर. सी. मॉडल का उपयोग यह जांचने के लिए किया जाता है कि यास चक्रवात के दौरान भूमि की सतह की विशेषताएँ सी. एफ. को कैसे प्रभावित करती हैं। इस मॉडल में भारत के पूर्वी तट के साथ ब्राह्मणी, बैतरणी, सुवर्णरेखा और महानदी नदी की सहायक नदियाँ शामिल हैं। सी. एफ. का अनुमान आई. एम. डी. ए. ए., ई. आर. ए. 5, जी. पी. एम. पी. सी. पी., वाष्पीकरण के साथ-साथ मिट्टी की घुसपैठ का उपयोग करके लगाया जाता है। उपग्रह छवि के साथ बाढ़ की सीमा के सत्यापन से पता चलता है कि पी. सी. पी. सी. एफ. का प्रमुख कारण है। चूंकि घुसपैठ की दर मुख्य रूप से मृदा संरक्षण सेवा वक्र संख्या (एससीएन) और न्यूनतम घुसपैठ दर पर निर्भर करती है, इसलिए संवेदनशीलता विश्लेषण से पता चलता है कि न्यूनतम मिट्टी की घुसपैठ और अधिकतम एससीएन कम जल प्रवेश और उच्च अपवाह के कारण बाढ़ को बढ़ाते हैं। उपयुक्त न्यूनतम घुसपैठ दर और एससीएन मूल्यों पर विचार करके टिप्पणियों के साथ जिलेवार बाढ़ को मापने के लिए प्रयोग किए जाते हैं, जिससे सीएफ में 50% की वृद्धि होती है। दो और ऐतिहासिक चक्रवातों (ओडिशा सुपर साइक्लोन और फेलिन) के साथ अतिरिक्त सिमुलेशन दर्शाते हैं कि पीसीपी का समावेश आरडी और एसटी फोर्सिंग की तुलना में बाढ़ को दोगुना कर देता है। यह कार्य सी. एफ. के लिए विभिन्न जिम्मेदार कारकों के महत्व के साथ-साथ इसमें शामिल अनिश्चितताओं को उजागर करता है और इसे और बेहतर बनाने के लिए संभावित समाधानों पर जोर देता है।

सी. एफ. के विभिन्न चालकों का सापेक्ष योगदान और भूमि-सतह प्रक्रियाओं के साथ उनकी बातचीत अभी भी स्पष्ट नहीं है, विशेष रूप से बेसिन आकृति विज्ञान के साथ विभिन्न मौसमों में। पारंपरिक हाइड्रोडायनामिक मॉडल आमतौर पर पीसीपी डेटा की कमी के कारण अपने प्रतिनिधित्व को अलग करते हैं जिसके परिणामस्वरूप जलप्लावन की कम भविष्यवाणी होती है। इस अंतर को भरने के लिए, भारत के पूर्वी तट के साथ तीन प्रमुख नदी नेटवर्कों पर एक पूरी तरह से युग्मित हाइड्रोलिक, हाइड्रोडायनामिक और पवन तरंग (एडीसीआईआरसी + स्वान + एचईसी-आरएएस) मॉडलिंग ढांचे का उपयोग किया जाता है: हुगली, महानदी-ब्राह्मणी-बैतरणी-सुवर्णरेखा और कृष्णा-गोदावरी बेसिन, सीएफ पर एसटी, आरडी, पीसीपी और सतह प्रक्रियाओं के संयुक्त प्रभावों की मात्रा निर्धारित करने के लिए। तट के साथ मानसून से पहले और बाद की चक्रवात अवधि के दौरान बहु-बेसिन और मौसमी रूप से स्तरीकृत महासागर में यह पहला अध्ययन है। सिमुलेशन से पता चलता है कि मॉडल हवाएँ और कुल पानी की ऊँचाई अवलोकनों के साथ मेल खाती है। अध्ययन से पता चलता है कि प्री-

मानसून सीएफ मुख्य रूप से पीसीपी के कारण होता है, लेकिन पोस्ट-मानसून सीएफ उच्च आरडी, पीसीपी और एसटी का एक यौगिक प्रभाव है। इसके अलावा, संवेदनशीलता विश्लेषण दर्शाता है कि नदी पार-अनुभागीय डेटा का सटीक प्रतिनिधित्व बहुत महत्वपूर्ण है, जबकि डिफ़ॉल्ट स्थलाकृतिक डेटासेट बाढ़ के विस्तार को अधिक महत्व देते हैं। मॉडल में मिट्टी की घुसपैठ की गतिशीलता का समावेश 30-38% तक जलमग्न क्षेत्र को कम कर देता है, और इसलिए वास्तविक समय सिमुलेशन में विचार किया जाना अनिवार्य है। यह भी पता चलता है कि एक स्टैंडअलोन एडीसीआईआरसी + स्वान आरडी और पीसीपी के गैर-समावेश के कारण कुल बाढ़ को 47% कम करके आंकता है, पूरी तरह से एकीकृत मॉडलिंग की आवश्यकता पर जोर देने वाले पूरी तरह से युग्मित दृष्टिकोण की तुलना में। अध्ययन डेटा और पद्धतिगत मुद्दों से संबंधित बाधाओं और पूरी तरह से युग्मित ढांचे से जुड़ी अनिश्चितताओं और इसे कम करने के संभावित तरीकों पर भी प्रकाश डालता है।

कुल मिलाकर, यह शोध प्रबंध भारतीय पूर्वी तट पर चक्रवात से उत्पन्न बाढ़ का बहु-स्तरीय मूल्यांकन प्रदान करता है। यह इस बात की समझ को आगे बढ़ाता है कि कैसे सतह और तल का तनाव, तटरेखा विन्यास, भूमि-सतह की विशेषताएँ, और बहु-चालक अंतःक्रियाएँ जलप्लावन के स्थानिक और लौकिक विकास को आकार देती हैं। इन निष्कर्षों का तटीय क्षेत्र प्रबंधन, आपदा तैयारियों और चक्रवात-प्रवण क्षेत्रों में लचीले तटीय बुनियादी ढांचे के विकास के लिए मजबूत प्रभाव पड़ता है।

Table of Contents

Certificate	
Acknowledgements	
Abstract	i-viii
Table of Contents	ix-xv
List of Figures	xvi-xx
List of Tables	xxi-xxii
Chapter 1 INTRODUCTION	1-28
1.1 Background of the Study	1
1.2 Tropical Cyclones	3
1.2.1 Cyclones in the north Indian Ocean	6
1.3 Storm Surges, Storm Tides, and Total Water Elevations	9
1.4 Review of Storm Surge Modelling in the Bay of Bengal	12
1.5 Coastal Inundation due to Cyclonic Storms	14
1.6 Effect of Compound Flooding (CF)	16
1.7 Gaps in the Research Area	18
1.8 Scope of the Present Study	20
1.9 Novelty of the Present Study	21
1.10 Objective of the Study	23
1.11 Outline of the Thesis	24
Chapter 2 CONFIGURATION OF THE ADCIRC MODEL FOR THE EAST COAST OF INDIA TO COMPUTE TIDES AND STORM SURGES IN RESPONSE TO TROPICAL CYCLONES AND ITS VALIDATION	29-50
2.1 Introduction	29
2.2 Description of ADCIRC Model	31

2.2.1	Governing equations	32
2.2.2	Boundary conditions	34
2.2.3	Tidal forcing	36
2.2.4	Wetting and drying scheme	37
2.3	Cyclone Wind Module	38
2.4	The Wind Wave Model: SWAN	40
2.5	Coupling of ADCIRC and SWAN	42
2.6	Model Setup and Configuration	43
2.7	Validation of Tides	45
2.8	Description of the HEC-RAS Model	47
2.9	Coupling of ADCIRC+SWAN+HEC-RAS Model	49
2.10	Conclusions	50
Chapter 3	ASSESSMENT OF THE LULC IMPACT ON CYCLONIC WINDS AND ASSOCIATED COASTAL INUNDATION	51-76
3.1	Introduction	51
3.2	Synoptic History of Cyclones	54
3.2.1	Thane cyclone	54
3.2.2	Titli cyclone	54
3.2.3	Fani cyclone	54
3.2.4	Bulbul cyclone	55
3.3	Model Description	55
3.3.1	Hydrodynamical surge model	55
3.3.2	Holland wind module	55
3.4	Data and Methodology	56
3.4.1	Data	56
3.4.2	Model mesh	56

3.4.3	Incorporation of surface roughness length and manning's n value in the model	57
3.4.4	Model simulations	60
3.5	Results and Discussion	61
3.5.1	Observational analysis	61
3.5.2	Model Simulations	62
3.5.2.1	Wind speed validation	63
3.5.2.2	Tide-gauge validation	66
3.5.2.3	Computation of coastal inundation	67
3.5.2.4	Sensitivity experiments with LULC	71
3.6	Conclusions	75
Chapter 4	IMPACT OF COMPLEX COASTLINE GEOMETRY ON THE EVOLUTION OF STORM SURGES ALONG THE EAST COAST OF INDIA: A SENSITIVITY STUDY USING THE ADCIRC MODEL	77-111
4.1	Introduction	77
4.2	Synoptic History of the Michaung Cyclone	80
4.3	Model Description	81
4.3.1	ADCIRC model	81
4.3.2	Holland wind module.	81
4.4	Data and Methodology	82
4.4.1	Experiments using cyclone Michaung (Exp1)	82
4.4.2	Experiments using idealized coastline (Exp2)	82
4.4.2.1	Calculation of angles with respect to maximum peak surges (MPS) location based on the shape of the domain	85
4.4.3	Experiments using real coastline (Exp3)	86
4.5	Results and Discussion	87

4.5.1	Computation of storm tides for the Michaung cyclone	87
4.5.2	Peak surge generation with parallel cyclone racks in the idealized domains	89
4.5.3	Onshore and alongshore winds	95
4.5.4	Generation of positive and negative surges along the coast	98
4.5.5	Computation of energy density per unit length of a surge wave in the concave coast	100
4.5.6	Computation of peak surges by parallel tracks using actual stretch along the east coast of India	102
4.5.7	Computation of peak surges by the tracks with different approach angles using actual coastal stretch along the east coast of India	104
4.5.8	Computation of peak surges by parallel tracks with different Rmax using actual coastal stretch along the east coast of India	106
4.6	Conclusions	108
Chapter 5	EFFECT OF LAND SURFACE PARAMETERS ON COASTAL INUNDATION USING A COUPLED HYDRAULIC AND HYDRODYNAMIC MODEL: A CASE STUDY WITH A MAJOR RIVER BASIN	112-144
5.1	Introduction	112
5.2	Synoptic History of Yaas Cyclone	115
5.3	Model Description	115
5.3.1	Hydrodynamic surge model (ADCIRC)	115
5.3.2	Hydraulic model (HEC-RAS)	116
5.4	Data and Methodology	116

5.4.1	ADCIRC model	116
5.4.2	HEC-RAS model	116
5.4.3	Coupling methodology	123
5.4.4	Calibration, validation and sensitivity framework. of coupled modelling framework	124
5.5	Results and Discussion	124
5.5.1	Cyclonic wind and surge residual validation	124
5.5.2	Computed inundation from the sentinel and the model	126
5.5.3	Computed inundation using precipitation, evaporation from IMDAA, ERA5, and GPM	128
5.5.4	Contribution of precipitation, evaporation, and storm tides on inundation using IMDAA and ERA5	132
5.5.5	Sensitivity analysis using different soil parameters with IMDAA Data	135
5.5.6	Computed inundation from the calibrated model	137
5.5.7	Comparison of compound flooding during different cyclones	140
5.6	Conclusions	142
Chapter 6	AN INTEGRATED MODELLING APPROACH FOR REALISTIC SIMULATIONS OF COMPOUND FLOODING ALONG THE EAST COAST OF INDIA	145-178
6.1	Introduction	145
6.2	Synoptic History of Cyclones	148
6.2.1	Amphan cyclone	148
6.2.2	Bulbul cyclone	148

6.2.3	Fani cyclone	148
6.2.4	Phailin cyclone	148
6.2.5	Laila cyclone	149
6.2.6	Lehar cyclone	149
6.3	Model Description	149
6.3.1	Hydrodynamic surge model (ADCIRC)	149
6.3.2	Wave model (SWAN)	150
6.3.3	Hydraulic model (HEC-RAS)	150
6.4	Data and Methodology	150
6.4.1	Coupled ADCIRC and SWAN model configuration	150
6.4.2	HEC-RAS model configuration	151
6.4.3	Methodology of the coupled model	156
6.5	Results and Discussion	157
6.5.1	Cyclonic wind and surge residual validation	157
6.5.2	Precipitation and evaporation during the cyclone period	161
6.5.3	Upstream river discharge during cyclone period	164
6.5.4	Sensitivity experiments using pre- and post-monsoon River Discharge along with change in the river cross-sections	166
6.5.5	Contribution of precipitation, river discharge, and storm tides in the coastal inundation	168
6.5.5.1	Hooghly basin (Amphan: pre-monsoon, Bulbul: post-monsoon)	168
6.5.5.2	MBBS basins (Fani: pre-monsoon,	169

Phailin: post-monsoon)	
6.5.5.3 K-G basins (Laila: pre-monsoon, Lehar: post-monsoon)	169
6.5.6 Contribution of soil infiltration to the coastal inundation	172
6.5.7 Inundation due to coupled ADCIRC+SWAN model	174
6.6 Conclusions	176
Chapter 7 CONCLUSIONS AND FUTURE SCOPE OF THE WORK	179-186
7.1 General Conclusions	179
7.2 Future Scope of the Work	184
References	187-201
List of Acronyms	202-204
List of Symbols	205-208
List of Websites	209
Biographical Sketch	210-213

List of Figures

Figure No.	Title	Page No.
Fig. 1.1	Vertical cross-section of a tropical cyclone.	4
Fig. 1.2	Cyclones, Hurricanes, and Typhoons with their peaks of activity worldwide.	6
Fig. 1.3	Cyclonic storms and severe cyclonic storms developed during the post-monsoon season (1891-2024) in NIO.	8
Fig. 1.4	Illustration of the impact of the tide on storm surge levels.	11
Fig. 1.5	East coast of India along with major river systems.	15
Fig. 1.6	Components of compound flooding: (a) Fluvial floods, (b) Pluvial floods, and (c) Coastal floods.	17
Fig. 1.7	Different factors responsible during compound flooding.	18
Fig. 2.1	Computational domain along with tide-gauge stations.	44
Fig: 2.2	Comparison of modelled tide against the observed tide at (i) Dhamra, (ii) Krishnapatnam, (iii) Paradeep, (iv) Kakinada, (v) Visakhapatnam and (vi) Ennore tide-gauge locations.	46
Fig: 2.3	Workflow of coupled ADCIRC_SWAN_HEC-RAS model.	49
Fig. 3.1	Model domain along with cyclone tracks of Bulbul, Fani, Titli and Thane.	57
Fig. 3.2	ERA5 wind speed over the land and ocean at the time of landfall for the cyclones: (a) Bulbul, (b) Fani, (c) Titli and (d) Thane.	62
Fig. 3.3	Model wind speed over land and ocean at the time of landfall for the cyclone Fani. (a) Without LULC and (b) With LULC. Boxes represent selected areas over land and the ocean. Zoomed inset images to highlight changes in wind speed over the land without and with LULC.	64
Fig. 3.4	ASOS wind speed (blue) and model wind speed without LULC (green) and with LULC (red) for the cyclones: (a) Bulbul, (b) Fani, (c) Titl and (d) Thane. Black dot shows the cyclone landfall time.	65
Fig. 3.5	Comparison of modeled ST and surge residual against the observed ST and surge residual at (a) Paradeep for cyclone Fani and (b) Ennore for cyclone Thane. The black dot shows the cyclone's landfall time.	66

Fig. 3.6	Depiction of maximum water levels and associated coastal inundation during Bulbul cyclone along with its track (a) without LULC and (b) with LULC. Zoomed inset to highlight the area with maximum water levels.	67
Fig. 3.7	Depiction of maximum water levels and associated coastal inundation for Fani cyclone along with its track (a) without LULC and (b) with LULC. Zoomed inset to highlight the area with maximum water levels.	68
Fig. 3.8	Depiction of maximum water levels and associated coastal inundation for Titli cyclone along with its track (a) without LULC and (b) with LULC. Zoomed inset to highlight the area with maximum water levels.	69
Fig. 3.9	Depiction of maximum water levels and associated coastal inundation for Thane cyclone along with track (a) without LULC and (b) with LULC. Inset images are zoomed to highlight the area with maximum water levels in both the domains.	70
Fig. 3.10	Existing wetland area (grey colored) in the Krishna estuary. Arrows in yellow color show the maximum wetland extent from the coast. A hypothetical cyclone track is shown on left of the estuary (red color).	72
Fig. 3.11	Wind speed at the time of landfall in the Krishna estuary with (a) wetland and (b) mangroves. Zoomed inset to highlight the changes in wind speed over the estuary after considering wetlands into mangroves.	73
Fig. 3.12	Coastal inundation in the Krishna estuary with (a) wetland (b) mangroves when considered both surface and bottom friction (c) mangroves when considered only surface friction and having same bottom friction as in the case of wetland. Zoomed inset to highlight the inundated areas.	74
Fig. 4.1	Michaung cyclone track and its intensity with time.	81
Fig. 4.2	Model domain along with different coastline geometry (zoomed).	83
Fig. 4.3	(i) Parallel tracks used in the study. Black dot represents the vertex of the domain. (ii-vii) Shapes of idealized coastlines considered for concave (CC1-CC6), (viii-xiii) convex (CV1-CV6), and (xiv) straight coastlines.	84
Fig. 4.4	Angle of a tangent (θ) to an ellipse at the point of maximum peak surge (MPS).	86
Fig. 4.5	(i) Model computed maximum storm tide for the Michaung cyclone. (ii) Comparison of model and tide-gauge data at Krishnapatnam.	88

Black vertical line represents landfall time.

Fig. 4.6	Generation of maximum peak surge (MPS) for all the cyclone tracks for (i) concave and (ii) convex coastlines and due to different tracks within the (iii) concave and (iv) convex curvatures.	89
Fig. 4.7	Peak surge generated along the coast for two distinct shapes of concave (CC1 and CC6) and convex (CV1 and CV6) coastlines. Numbers inside the plot represent tangent angle (θ) to the location of peak surge.	94
Fig. 4.8	Time series of onshore and alongshore cyclonic wind components for (i-ii) CC1, (iii-iv) CC6, (v-vi) CV1 and (vii-viii) CV6. Black vertical line represents the landfall time.	96
Fig. 4.9	(i-xx) Time of occurrence of surges along the coast with reference to the landfall location for CC1, CC6, CV1 and CV6 for all the tracks. Black vertical line represents the landfall time.	99
Fig. 4.10	Energy propagation associated with the peak surge for (i) CC1 and (ii) CC6 as the cyclone proceeds towards the coast. The L refers to the cyclone landfall.	101
Fig. 4.11	Occurrence of peak surge along the actual concave coastline with the different parallel cyclonic tracks landfalling at (i) west (Track 1), (ii) center (Track 2) and (iii) east (Track 3) of the concave coastline.	103
Fig. 4.12	Effect of approach angle (45 (track 1), 165 (track 2) and 180 degree (track 3)) on peak surges due to tropical cyclone landfalling at (i-iii) west, (iv-vi) center and (vii-ix) east of the concave coastline.	105
Fig. 4.13	The occurrence of peak surge over concave coastline with different parallel tracks and radius of maximum wind (R_{max}) of (i-iii) 20km, (iv-vi) 30km and (vii-ix) 40km.	107
Fig. 5.1	(a) HEC-RAS model domain with modified and unmodified river cross-sections along with the upstream river discharge and downstream storm tide points. (b) ADCIRC model domain along with Yaas cyclone track used in the study.	117
Fig. 5.2	(a-e) Unmodified and modified SRTM river cross-sections at the upstream river discharge locations and (f-l) at the downstream storm tide-gauge locations.	118
Fig. 5.3	(a) Soil type and (b) Land use and land cover type over the study area.	120
Fig. 5.4	Flow chart of the workflow used in the study.	123
Fig. 5.5	(a) Comparison of observed and modeled water level at Dhamra port. (b) Computed surge residual and (c) Wind speed validation at buoy	125

location (BD08, BD09, and BD10) for the Yaas cyclone. The black dot represents landfall time.

Fig. 5.6	(a,d) Satellite calculated inundation, and model calculated inundation (b,e) with default configuration and (c,f) using average values of minimum infiltration rate for the Yaas cyclone.	128
Fig. 5.7	IMDAA, ERA5, and GPM precipitation (a-i) and evaporation (j-o) during 24 - 26 May.	130
Fig. 5.8	(a-c) IMDAA, ERA5, and GPM calculated inundated on 26 th - 28 th May and (d) Satellite, IMDAA, ERA5, and GPM calculated inundated on May 29.	132
Fig. 5.9	(a-d) Contribution of precipitation, evaporation, and storm tide from 26 th – 29 th May for IMDAA and ERA5.	134
Fig. 5.10	Calculated inundation for (a) default SCN and high minimum infiltration rate, (b) default SCN and low minimum infiltration rate, (c) high SCN and low minimum infiltration rate, and (d) difference between different sensitivity experiments.	136
Fig. 5.11	Calculated inundation for (a and d) Satellite, (b and e) Default configuration, (c and e) Final calibrated products, district-wise inundation for (g) updated je minimum infiltration, and (h) Final values.	139
Fig. 5.12	Inundated area due to different flood drivers (river discharge, precipitation and storm tides) for the cyclones (a,d) Yaas, (b,e) OSC and (c,f) Phailin.	141
Fig. 6.1	HEC-RAS model domain with modified river cross-sections along with the upstream river discharge (black dot) and downstream storm tide points (white line) for (a) Hooghly, (b) MBBS, and (c) K-G. (d) ADCIRC+SWAN model domain along with cyclone tracks used in the study.	152
Fig. 6.2	(a-q) Modified and un-modified river cross-sections at upstream and downstream river points for Hooghly basin.	153
Fig. 6.3	(a-l) Modified and un-modified river cross-sections at upstream and downstream river points for the Mahanadi-Brahmani-Baitarani-Subarnarekha basins.	154
Fig. 6.4	(a-k) Modified and un-modified river cross-sections at upstream and downstream river points for the Krishna-Godavari basins.	154
Fig. 6.5	(a) Major coastal districts affected during cyclones, (b) Land use and land cover type, and (c) soil classifications over the study area.	155
Fig. 6.6	Flow chart of the workflow used in the study.	157

Fig. 6.7	(a-i) Comparison of observed and modeled wind speed at different buoy locations and cyclones. The black dot represents the landfall time.	159
Fig. 6.8	(a-i) Comparison of observed and modelled total water level at different tide-gauge locations for different cyclones. The black dot represents the landfall time.	161
Fig. 6.9	IMDAA precipitation and evaporation for the pre- and post-monsoon cyclones during the cyclonic period. Red line depicts the cyclone track.	163
Fig. 6.10	River discharge at upstream river points for pre- and post-monsoon cyclones during the cyclonic period.	165
Fig. 6.11	Coastal inundation due to precipitation, river discharge and storm tides for Phailin cyclone using pre-monsoon river discharge (a-d) and post-monsoon river discharge (e-h) along default and modified cross-sections. Black line depicts cyclone track.	167
Fig. 6.12	Coastal inundation due to precipitation, river discharge and storm tide for (a,b) Amphan, (c,d) Bulbul, (e,f) Fani, (g,h) Phailin, (i) Laila and (j,k) Lehar cyclones. Black line depicts cyclone track.	171
Fig. 6.13	Coastal inundation considering with and without soil infiltration in the model for (a,b) Amphan, (c,d) Bulbul, (e,f) Fani, (g,h) Phailin, (i,j) Laila and (k,l) Lehar cyclones. Black line depicts cyclone track.	173
Fig. 6.14	Computed coastal inundation using coupled ADCIRC+SWAN model for the cyclones (a) Amphan, (b) Laila, (c) Bulbul, and (d) Lehar. The black line depicts cyclone track.	175

List of Tables

Table No.	Title	Page No.
Table 1.1	Classification of cyclonic disturbance according to IMD.	5
Table 2.1	Datasets and their spatial resolution used to prepare the geometry of the domain.	44
Table 2.2	Correlation coefficient and RMSE at different tide-gauge locations.	46
Table 3.1	Manning's n coefficient and surface roughness length based on MODIS LULC data.	59
Table 3.2	Statistical analysis on winds along with its comparison using ASOS and model for different cyclones.	65
Table 4.1	Detail of the experiments used in the study.	86
Table 4.2	Maximum peak surge along with the tangent angle at Rmax for the different tracks for the concave shape.	91
Table 4.3	Maximum peak surge along with the tangent angle at Rmax for the different tracks for the convex shape.	92
Table. 4.4	Onshore and alongshore wind for different tracks for the shapes CC1, CC6, CV1 and CV6.	97
Table 4.5	Maximum peak surge along with the tangent angle at Remix for the different tracks for the convex shape.	101
Table 5.1	Manning's n and impervious percentage of the different land classifications of Sentinel LULC data.	119
Table 5.2	Range of infiltration rate for the different soil classification.	120
Table 5.3	SCN number based on different LULC and soil categories.	121
Table 5.4	Statistical analysis on buoy and model computed winds.	126
Table 5.5	Final calibrated soil parameters for each district.	139
Table 6.1	Range of infiltration rate for the different soil classifications.	155
Table 6.2	Statistics of model computed wind speed and TWL with observations.	159

Table 6.3 Percentage of total inundated area attributable to the RD_ST scenario vs. the Pcp_RD_ST scenario.

171